



HAL
open science

Simultaneous doping of sulfur and chloride ions into ZnO nanorods for improved photocatalytic properties towards degradation of methylene blue

Zaheer Ahmed Ujjan, Muhammad Ali Bhatti, Aqeel Ahmed Shah, Aneela Tahira, Nek Muhammad Shaikh, Shusheel Kumar, Abdul Qayoom Mugheri, Shymaa S Medany, Ayman Nafady, Fahad Alnjiman, et al.

► To cite this version:

Zaheer Ahmed Ujjan, Muhammad Ali Bhatti, Aqeel Ahmed Shah, Aneela Tahira, Nek Muhammad Shaikh, et al.. Simultaneous doping of sulfur and chloride ions into ZnO nanorods for improved photocatalytic properties towards degradation of methylene blue. *Ceramics International*, 2021, 10.1016/j.ceramint.2021.11.098 . hal-03428810

HAL Id: hal-03428810

<https://hal.univ-lorraine.fr/hal-03428810>

Submitted on 15 Nov 2021

HAL is a multi-disciplinary open access archive for the deposit and dissemination of scientific research documents, whether they are published or not. The documents may come from teaching and research institutions in France or abroad, or from public or private research centers.

L'archive ouverte pluridisciplinaire **HAL**, est destinée au dépôt et à la diffusion de documents scientifiques de niveau recherche, publiés ou non, émanant des établissements d'enseignement et de recherche français ou étrangers, des laboratoires publics ou privés.



Distributed under a Creative Commons Attribution - NonCommercial - NoDerivatives 4.0 International License

Simultaneous doping of sulfur and chloride ions into ZnO nanorods for improved photocatalytic properties towards degradation of methylene blue

Zaheer Ahmed Ujjan^a, Muhammad Ali Bhatti^c, Aqeel Ahmed Shah^e, Aneela Tahira^b, Nek Muhammad Shaikh^a, Shusheel Kumar^a, Abdul Qayoom Mugheri^b, Shymaa S. Medany^g, Ayman Nafady^d, Fahad Alnjiman^f, Mélanie Emo^f, Brigitte Vigolo^f, Zafar Hussain Ibupoto^b

^aInstitute of Physics University of Sindh Jamshoro, 76080, Sindh Pakistan

^bDr. M.A Kazi Institute of Chemistry University of Sindh Jamshoro, 76080, Sindh Pakistan

^cInstitute of Environmental Sciences, University of Sindh Jamshoro, 76080, Sindh Pakistan

^dDepartment of Chemistry, College of Science, King Saud University, Riyadh 11451, Saudi Arabia

^eNED University of engineering and Technology Karachi, Pakistan

^fUniversité de Lorraine, CNRS, IJL, F-54000 Nancy, France

^gChemistry Department, Faculty of Science, Cairo University, Cairo, Egypt

***Corresponding authors.** Zafar Hussain Ibupoto, & Ayman Nafady

Email: zaffar.ibhupoto@usindh.edu.pk, anafady@ksu.edu.sa (AN)

Abstract

In this study, we have successfully doped sulfide (S^{2-}) and chloride (Cl^{-1}) simultaneously into ZnO by hydrothermal method. The structure, morphology, composition and optical properties of the prepared S-Cl doped ZnO nanostructures were investigated by x-ray diffraction (XRD), scanning electron microscopy (SEM), scanning transmission electron microscopy (STEM), energy dispersive spectroscopy (EDX) and UV-visible (UV-Vis) spectroscopy techniques. After, doping of both S and Cl into ZnO no significant alteration in the nanorod morphology was noticed. The wurtzite crystal structure of ZnO was

retained with a red shift in the 2θ towards high angle. The XRD results are supported by the high resolution transmission electron microscopy. The elemental analysis revealed a successful doping of S and Cl into ZnO structure. Importantly, the optical band gap of ZnO was decreased 2.9 eV upon doping of S and Cl ions. Thus, the nonmetal doping via S and Cl has significantly enhanced the photocatalytic properties of ZnO towards methylene blue (MB) due to high density of active sites and decreased charge recombination rate of electron-hole pairs. The photo-degradation efficiency towards MB reached 99.64% upon using S and Cl doped ZnO photocatalyst using optimum dose of 15 mg and initial dye concentration of $1.87 \times 10^{-6} \text{M}$. The use of simultaneous nonmetal doping concept could of great importance for the preparation of other nanostructured materials and their use in potential applications like solar cells, and photoelectrochemical water splitting.

Keywords: Nonmetal dopant, ZnO, Methylene blue, photodegradation

1. Introduction.

Over the recent years, the textile industry is one of the most pollutants releasing industry into the environment. These pollutants contain a heavy load of chemicals including dyes and they have been cause of harming our environment. These dyes are found at large quantities into the waster of textile industry which not only affect the human life but as well as aquatic life. Furthermore, these dyes exist in various forms such as an acidic, disperse, fabric, mordant, reactive, vat, and ingrain azo. These dyes are found as colored in the wastewater. The structural information of dyes tells that they contain an aromatic ring in their structure, and they can be dissolved either into organics or inorganic solvents and they can be found as suspended solids which are supposed to

be cause of toxicity. These colored substances cause serious health problems including skin disease, allergy, cancer and mutation. These substances are not only affecting the human organs such as kidney, liver, central nervous system and brain, but also at the same to the aquatic life by acting as shield for the sunlight and thereby resisting the access of light to aquatic life. In addition, the survival of human and aquatic life in their ecosystem is probably impossible without the availability of pure water to them. The inappropriate disposal of by-products and an excessive use of chemicals into the industry have degraded the quality of natural water [01-03]. The methylene blue (MB) discharged by the dying industries is one of the most prominent dye among the different dyes. For the removal of MB various methods such as reverse osmosis, adsorption on activated carbon, coagulation, poly-electrolyte promoted, nano-filtration, electrochemical treatment, biological treatment in particularly enzyme and photo-catalytic degradation have been employed [04]. Photocatalytic degradation is one of the most competitive methods which effectively solve the degradation issue of dyes from wastewater and it has several advantages including simplicity, efficient, and do not produce secondary pollutants [5]. The photocatalytic method requires a high energy light irradiation source and an oxidant to generate hydroxyl radicals which are involved degradation process. All the renewable technologies have attracted huge attention because they offer promising results and can be used as potential alternative for the energy generation and wastewater treatments. Photocatalysis is supposed to be an efficient technique to degrade the recalcitrant wastewater [6]. Many researchers reported the use of semiconducting materials (TiO_2 , CdS , ZnO , WO_3 , Fe_2O_3 , SnO_2 etc) as photocatalyst or the wastewater treatments [7–12]. Among the various semiconductor materials, ZnO is generally considered as a good photocatalyst for the degradation of organic dyes due to its stability in chemicals properties, non-toxicity and inexpensiveness [13]. However, some major drawbacks including its wide band gap 3.37 eV (bulk) which may limit the absorption of light in the ultraviolet region and fast rate of electron-hole recombination rate which severely affects the performance of ZnO as photocatalyst. Therefore, the development of efficient and stable photocatalysts based on ZnO for the practical applications are highly needed. We need to utilize the large region of solar spectrum and to overcome the recombination rate of electron and hole pairs. These are the main challenges in the current state of art of photocatalysts based on ZnO [14]. The photo-response of ZnO may be enhanced in the visible spectrum of solar light by employing various alternative strategies including doping into ZnO , co-doping, coupling with lower band semiconductors, surface plasmon response, quantum

dots, sensitization with natural and synthetic dyes [15-31]. Doping is known as the suitable approach to increase the optical spectrum and catalytic properties [32, 33]. The literature survey shows that some nonmetal dopants like (*e.g.* carbon (C), nitrogen (N), and sulfur (S)) into ZnO cause the creation of intermediate or lower energy levels between the band gap, enabling ZnO to absorb visible light and minimize the recombination rate of electron-hole pairs due to photo-excited electrons to nanosized nonmetal atoms on the surface of the catalyst, therefore efficiently degraded the dyes in the wastewater [34-36]. The use of S and Cl separately as nonmetal dopant into ZnO has been carried out, however the simultaneous doping of S and Cl into ZnO is not reported elsewhere.

In this study, the doping of S and Cl into ZnO simultaneously has been studied for the photodegradation of MB. The doping of S and Cl into ZnO has been carried out by hydrothermal method. The structural studies of doped samples were carried out by SEM, XRD, HRTEM and EDS techniques. The optical characterization on the nonmetal doped ZnO was studied by UV-visible spectroscopy. The performance of doped samples was found very efficient for the degradation of MB and efficiency of 99.66 % is reported herein.

2. Experimental Methodology

2.1 Materials

The chemicals use in this study include ammonium sulphide $(\text{NH}_4)_2\text{S}$ or $\text{N}_2\text{H}_8\text{S}$, ammonium chloride (NH_4Cl), sodium hydroxide (NaOH), zinc acetate-dihydrate ($\text{ZnC}_4\text{H}_6\text{O}_4$), 25% aqueous ammonia solution Merck), methylene blue ($\text{C}_{16}\text{H}_{18}\text{N}_3\text{SCl}$) organic dye, and ethanol ($\text{C}_2\text{H}_5\text{OH}$, 99.5%) were purchased from Sigma-Aldrich Karachi, Pakistan and used without further purification. The deionized water (DI) was used in all the experiments.

2.2 Synthesis of simultaneously S and Cl doped ZnO nanorods by hydrothermal method

The hydrothermal method was employed for the synthesis of ZnO and S as well as Cl doping ZnO nanostructures. We used zinc acetate di-hydrate ($\text{ZnC}_4\text{H}_6\text{O}_4$) and 25 % ammonia for the fabrication of ZnO. The 0.01 M concentration of ammonium chloride and 0.01 M concentration of ammonium sulphide, 0.1 M of sodium hydroxide and 0.1 M of zinc acetate di-hydrate were mixed in equal

volume of ethanol and deionized water and their well dispersion was obtained by employing ultrasonic bath for 30 min. The pristine ZnO was prepared by same method by dissolving 0.1 M zinc acetate di-hydrate and 0.1M NaOH. The aluminum foil was employed to seal the beakers in order to avoid the evaporation of aqueous solution during hydrothermal process. The growth process was carried out in preheated electric oven at 90 °C for 5 h. Finally, filtration and drying processes were employed to collect the white product of ZnO nanostructures.

X-ray diffraction was performed with powder diffractometer (D8 Advance, Bruker) employing the experimental conditions of CuK α radiation ($\lambda = 1.54050 \text{ \AA}$), 45 mA, 45 kV and at a scan rate of 1° min^{-1} . Scanning electron microscopy was carried out with a ZEISS Gemini SEM 500 equipped with field emission gun. The elemental analysis was determined by energy dispersive X-ray spectroscopy (EDS) embedded in the scanning electron microscope. The scanning transmission electron microscopy (STEM) observations were carried out with a JEOL ARM 200-Cold FEG at 80 kV along with energy dispersive X-ray (EDX). For the observations, the powder was dispersed in ethanol and a drop of the dispersion was deposit on a holey carbon grid (200 mesh size). The degradation rate and the quantitative decrease in the concentration of MB was quantified by a UV-visible spectrophotometer (PerkinElmer, Lambda 1050).

2.3. Photocatalytic Activity of prepared ZnO nanostructures

The photocatalytic activity of as synthesized ZnO nanostructures was investigated with the degradation of methylene blue (MB) dye using different dose concentrations 0.62×10^{-6} , 1.87×10^{-6} , 2.50×10^{-6} M in deionized water. Pristine and S-Cl doped ZnO nanostructures of 10 mg were placed horizontally in the two 100 mL beakers containing 1.87×10^{-6} M of MB dye and exposed to ultraviolet (UV) light. Typically the reaction suspension was prepared by adding different dose concentration of (5, 10, 15) mg of the as-prepared S-Cl-doped ZnO powders into 100 mL of 10 mg methyl blue aqueous solution. Before applying UV light, the aqueous suspension of stock solution containing different catalyst and MB (0.62×10^{-6} , 1.87×10^{-6} , 2.50×10^{-6} M) dye dose concentration placed in sonicator for 30 min for achieving adsorption-desorption equilibrium. Later on, the MB stock solution was irradiated with UV-Visible light under the room temperature. The UV-Visible light was employed for carrying out the degradation activity through locally made photoreactor using a compact UV lamp of (365 nm) and a power of 18 watt were applied. The UV-visible spectrophotometer (PE Lambda35) was employed to record the main absorbance peak

to quantify the MB dyes which detected at (664) nm. The UV–visible spectrophotometer recorded the absorption spectrum after every 30 min intervals to monitor the MB concentration in the stock solution. The intensity of absorption spectrum at characteristic wavelength of (664) nm was observed to determine the concentration of MB by recording UV visible spectra in the wavelength range of 200–800nm. The mathematical formula used for the calculation of decolorization efficiency for as synthesized intrinsic ZnO and S-Cl doped ZnO nanostructures was as follows:

$$\text{Degradation Efficiency (\%)} = \left(\frac{C_o - C_t}{C_o} \right) \times 100 \quad (1)$$

Where C_o (gm/L) is the initial dye concentration and C_t (gm/L) shows MB dye (mg/L) after certain interval of time.

3. Results and Discussions

3.1 Structural characterization of various ZnO nanostructures

The morphological investigations of pristine ZnO and S-Cl doped ZnO were evaluated by employing the scanning electron microscope. It is well observed through the SEM study that pristine ZnO and S-Cl-doped ZnO nanostructures have almost homogeneous morphology, however some randomly oriented particles are associated with the S and Cl doped sample as shown in Figure 1. The pristine ZnO exhibits well defined nanorod like morphology with random alignment. The length of ZnO nanorods could be few microns and the average diameter around 200 nm as shown in Figure 1a-b. The S and Cl doped ZnO sample possesses a heterogeneous morphology consisting nanorods and cluster of particles as shown in Figure 1c-d. The size of particles could be larger than 100 nm and the length of nanorods is decreased with the addition of S and Cl source due to etching effect.

EDX is a very reliable technique to quantitatively analyze the presence of zinc, oxygen, sulfur and chlorine in the S-Cl-doped ZnO sample as shown in Figure 2(a & b). The EDX patterns reveal only peaks at the energies of zinc and oxygen for pristine ZnO (Figure 4a), indicating clearly the purity of synthesized nanostructures as shown in Figure 2(a), while for S-Cl doped ZnO, the spectrum shows peaks corresponding to sulfur, chlorine, zinc and oxygen atoms (Figure 2b), confirming the successful doping of S-Cl atoms in the lattice of ZnO.

STEM High Angle Annular Dark Field (HAADF) images of hydrothermally synthesized pristine and S-Cl doped ZnO nanostructures are presented in Figures 3a and 4a respectively. Figure 3a shows that pristine ZnO possesses a rod-like structure with a length of several microns, as shown previously by SEM. The product obtained by addition of S and Cl as a dopant into ZnO is heterogeneous and consists of a mixture of nanorods and nano-platelets (Figure 4a). The length of nanorods decreases with the addition of S and Cl. X-maps of detected elements are shown on Figures 3b-c and 4b-d. These observations highlighted that sulfur is incorporated mainly in the nano-platelets. The chlorine is mainly shown by EDS via SEM analysis and the percent distribution of chlorine was not uniform throughout the sample.

The pristine ZnO and S-Cl doped ZnO nanostructures were characterized by powder XRD. Fig. 5(a, b) reveals that the powder X-ray diffraction detected the patterns within the range of 20- 79° for pristine ZnO and S-Cl doped ZnO nanostructures with a scanning step of 0.01°. The sharpness as well as absence of impurity indicates the high purity of as-synthesized nanomaterial. Furthermore, the sharp peaks may be related to the planes which measured at 2 theta angle of 31.86° (100), 34.54° (002), 36.32° (101), 47.62° (102), 56.66° (110), 62.96° (103), 66.44° (200), 68.04° (112), 69.18° (201), 72.34°(004), 76.76°(202) and showing the clear randomly oriented ZnO nanostructures [37]. The XRD results are according to the reported reference JCPDS card No. 01-075-1533, and could be assigned to the hexagonal wurtzite structure of ZnO [38]. However, the XRD results for the doped sample clearly indicates the increasing order in the red shift. The red shift of dominant peaks is observed at 2 θ angle of 31.24, 33.78 and 35.84 degree lying at plane (100), (002) and (101) respectively as depicted in Fig 5(b). The shift in S-Cl doped ZnO sample might effect on the optical and morphological properties. Furthermore, the increasing order was observed in lattice parameters a and c and volumes V in the doped ZnO nanostructures. The lattice parameters 'a' and 'c' value were observed larger in S-Cl doped ZnO as compared to pristine ZnO. The ratio of c/a was found 1.732 which is very close value with ideal value of 1.6. This increase in lattice parameters of S-Cl doped ZnO may be caused by addition of dopant whose ionic radii such as S($r=1.09 \text{ \AA}$), Cl($r=1.81 \text{ \AA}$) into pristine ZnO with atomic radii such as Zn(1.38 \AA) and O(1.40), resulting in expansion of the S-Cl-ZnO lattice structures [39]. In addition the doping of S-Cl into ZnO can further alter the distance in crystal structure as well as in diffraction angle. Moreover, the crystallite size of the as-prepared samples was evaluated from Scherer's relation [40].

$$D(nm) = \frac{K\lambda}{(FWHM)_{hkl} \cos(\theta)} \quad (2)$$

Whereas D represents crystalline size (nm), K denotes shape factor K= 0.94, λ depicts wavelength of X-Ray (nm), β indicate Full Width at Half Maximum (rad) and θ denotes Bragg Diffraction Angle (deg). The (hkl) denotes the Miller Indices. The findings regarding average value of crystalline size of pristine ZnO and S-Cl doped ZnO nanostructures were obtained 35.292 nm and 26.209 nm, respectively at the plane value of (100) and as in the case of (101) the 50.2117 nm reduced to 44.4225 nm and at the plane (110) it decreased from 42.159 nm to 23.496 nm. The smaller crystalline size also called particle size is proportional to the enhancement of specific surface area which leads to increase in the number of active surface sites. Furthermore these increased surface active sites may lead better photocatalytic performance. This makes the photogenerated charge carriers react with absorbed molecules to form hydroxyl and superoxide radicals. These values were obtained in decreasing order with incorporation of S-Cl as a dopant concentration into ZnO. The observed decreasing behavior of crystalline size could be attributed to the diffusion and growth impairment of ZnO crystal grains, which is caused by the replacement of oxygen ($r = 1.40 \text{ \AA}$) in ZnO with either of S ($r = 1.09 \text{ \AA}$) or Cl ($r = 1.81 \text{ \AA}$). Loan T. T. Nguyen et. al has also reported the decrease in crystalline size of La-doped ZnO nanostructures[41]. These size characteristic is an essential parameter for possibly improving the photocatalytic properties of S-Cl-doped ZnO nanostructures. These crystal structure parameters values are summed up in Table 1.

3.2. Optical properties of synthesized nanostructures

The exploration of optical properties of pristine ZnO and S-Cl doped ZnO nanostructures were carried out using UV-visible absorption spectroscopy. The UV-vis absorption spectrum whose wavelength range between (200–800 nm) was recorded as shown in Fig. 6(a)

The effect of incorporation of S-Cl as dopant into ZnO was carefully analyzed which depicted the change appears in absorption wavelength and it shifted to longer wavelength for S-Cl doped ZnO, which may be assigned to agglomeration of the nanostructures. The literature survey shows that the shifting of absorbance wavelength to larger wavelength is in line with reported work [41]. It is worth noting that the band gap energy is considered to be main indicator for the determining the

potential and for assigning the difference between conduction band (CB) and valence band (VB). Tauc-equation was used to evaluate the band gap energy (E_g)

$$(\alpha h\nu)^n = k(h\nu - E_g) \quad (3)$$

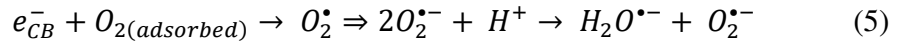
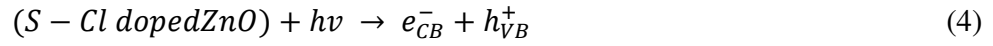
Whereas α , K , $h\nu$ represent the absorption coefficient, the energy-independent constant value, photon energy respectively and the optical band gap is denoted by E_g (e.V) and $n=2$. Tauc's plots of ZnO and S-Cl doped ZnO are represented in Fig 6(a-b). The insets in Fig 3(a-b) reveals the linear relation between $(\alpha h\nu)^2$ and $h\nu$ and this linear portion of Tauc's plot was extrapolated to the ordinate as to be equal to 3.24 eV. The addition of S-Cl as a dopant slightly reduces this value to 2.9 eV as shown in inset of Fig 3b, which reveals the ability of the synthesized nanostructures to harvest visible light. This band gap E_g value agrees with most of the reported studies about the nonmetal doped ZnO [34, 35, 42]. The decreased value of band gap was assigned to defect states between the conduction band and valence band of S-Cl-ZnO, which may possibly arise due to the interaction of S-Cl-doping into ZnO. Thus, the S-Cl doped ZnO results in decline in the optical band gap energy which might enhance the photocatalytic properties of S-Cl-ZnO nanostructures to perform efficient degradation of organic pollutants.

3.3. Photodegradation activity towards methylene blue

Fig. 7 shows the chemical structure of Methylene Blue (MB).

The undoped ZnO and S-Cl doped ZnO nanostructures were placed under UV light box locally made to irradiate UV radiation upon nanostructures to investigate the photocatalytic degradation of methyl blue (MB). The UV-visible spectra were recorded at different irradiation time intervals of 40 min for pure ZnO and 30 min for S-Cl-ZnO and presented in Fig 8(a), Fig 9(a-c) and Fig 10(a-c) respectively. The maximum absorbance peak at 664 nm was found in spectra of MB. The absorption of MB was decreasing at 664 nm which shows the function of irradiation time as shown in Fig. 8, 9 and 10. As soon as the surface area of ZnO and S-Cl doped ZnO nanostructures gets the illumination of UV light, it causes the ignition of photocatalytic decomposition process by generating the photo electron-hole pair between the conduction and valence bands, resulting in the degradation of organic compound. The photo-excited electron goes to CB and leaves behind a hole in valence band (VB). These electrons and holes exhibit the ability to offer high oxidation

potential to allow direct oxidation of MB in reaction medium. Furthermore, the recombination rate of electron and hole can be limited by the interactions of photogenerated species in VB and in CB by following the oxidation reaction with either H₂O, OH⁻ or O adsorbed on ZnO and S-Cl-ZnO to produce the hydroxyl radicals through the following reactions [40, 43]:



Finally the hydroxyl radicals are used as the scavengers to decompose MB dye pollutant through following reactions [43]



Fig:6(a) schematically reveals that the MB dye decreases slowly over the time of 150 min at the photocatalyst dose of 10 mg. Whereas in the case of S-Cl-doped ZnO the decreases the height of absorbance peak in concentration of the MB over the irradiation time 150 min as shown in Fig (9, 10). The photocatalytic degradation activity may be affected by various factors such as amount of catalysts, concentration of MB and radiation of energy and irradiation time. For the optimization of photocatalysis process, it is essential to study these parameters to observe their effect on photocatalytic degradation.

In order to determine the effect of photocatalyst amount on the degradation process, a series of experiments were carried out by varying the dose of S-Cl-ZnO 5, 10 and 15 mg for keeping constant dye concentration of MB $1.87 \times 10^{-6} \text{ M}$ constant. The pH of MB dye was kept constant 6.3 throughout the present study. De-colorization process was observed with decreasing absorbance of MB at different photocatalyst concentration as depicted in Figure 7. Fig 7 reveals that with

increasing photocatalyst from (5 - 15) mg the photocatalytic performance may be enhanced. The most efficient catalyst dose was 15 mg, and it resulted in about 99.66% degradation efficiency for the 1.87×10^{-6} M MB concentration over the time of 150 min as shown in Fig 11. The enhancement in the degradation performance of S-Cl doped ZnO may be attributed to creating the larger surface area, resulting in enhancing the absorption of UV light. The larger surface area leads to larger number of active sites, and these active sites are favorable for capturing the photogenerated electrons to improve the electron-hole separation efficiency and thereby improving the photocatalytic efficiency. The electrons and holes are responsible for the oxidizing water to generate the hydroxyl radicals $\bullet\text{OH}$, and $\bullet\text{O}^{2-}$ [44]. Our findings are in line with the reported works which show the enhancement in degradation efficiency of ZnO caused by enhanced free radical hydroxyl concentration [45-47]

The degradation of MB was carried out at various initial concentrations such as (0.62, 1.87 and $2.50) \times 10^{-6}$ M using pristine ZnO and S-Cl doped ZnO with dosage of 10 mg under UV irradiation. The obtained results revealed that the degradation efficiency and rate constant of MB with constant dosage of photocatalyst 10 mg was found in inversely relation with the initial concentration dye as shown in Fig 12. The decreased performance is shown the effect of varying MB dye concentration on photocatalytic performance may be assigned to increasing the adsorption of MB dye on the surface of S-Cl doped ZnO, resulting in reduction of $\bullet\text{OH}$ concentration on sites of catalyst [36, 48]. Beer-Lambert's law also supports the reverse relation between initial dye concentration and photocatalytic activity because the intensity of photons as well as the adsorption of photons on the surface of catalyst is limited which leading to the lowering the rate of photodegradation process. The degradation efficiency of 0.62×10^{-6} M MB concentration could reach up to the 93.46% with photocatalyst dosage of 10 mg over the same time of 150 min. Fig 12 (c) revealed that the minimum degradation efficiency could be achieved 65.56 % for 0.62×10^{-6} M MB with the photocatalyst dosage of 10 mg over the same time interval of 150 min. This low efficiency of the maximum MB dye concentration was assigned to lower penetration of photons to the surface of photocatalysts [49, 50].

The photocatalytic efficiency and degradation constant of pristine ZnO and S-Cl doped ZnO nanostructures for the degradation of methylene blue (MB) were performed in the presence of UV light at different time intervals of irradiation. The photocatalytic performance as well as the degradation rate is proportional to irradiation time interval and photocatalyst dosage. In order to confirming pseudo first-order kinetics, the MB solution was employed for the evaluation of in terms of quantifying the differences in degradation rates. The following equation can be used to deduce the photodecolorization rate constants Moreover, the rate of photocatalytic reaction and MB photodecolorization rate constants have been performed using pseudo first order kinetics as shown in the following equation.

$$\ln \frac{C_0}{C_t} = Kt \quad (12)$$

Whereas, C_0 shows initial concentration of MB C_t denotes concentration of MB at time (t), k shows Pseudo-first order degradation rate constant. A linearly fitting was employed over the quantity $\ln \frac{C_0}{C_t}$ versus time to determine the degradation rate coefficient. The obtained fitting results disclose that the apparent degradation rate coefficient varies significantly with addition of S and Cl ingredients into ZnO. Fig 8 (c) shows the linearly fitted kinetic plot between $\ln \frac{C_0}{C_t}$ and time interval (min) yielding the degradation rate coefficient to be equal to 0.00232 min^{-1} for pristine ZnO. The pseudo first order kinetics model is being followed by linearly fitted kinetic plot. Whereas in the case of S and Cl-doped ZnO provides greater degradation rate of MB. Fig 11(a) reveals the graph between (C_t/C_0) and time indicating the decreasing MB concentration at different time intervals. The degradation rate constants of S-Cl doped ZnO were evaluated by employing slope over graph $\ln \frac{C_0}{C_t}$ versus time at different loading of photocatalysts and MB keeping constant. It was found that the degradation rate constant could be equal to 0.00656 min^{-1} , 0.01003 min^{-1} , 0.03188 min^{-1} , indicating increasing trend with increasing the catalyst load as shown in Fig 13 (a). The obtained results resemble with the reported work and this effect was also observed by Sunil G. Shelar et al. in which degradation of MB (20 mg/L) was achieved 95% efficiency in the presence of the 1g/L Ag-doped ZnO over the time duration of 100 min [51]. The degradation efficiency of pure ZnO at $1.87 \times 10^{-6} \text{ M}$ of MB and 10 mg of catalyst was yielded the 42.35% over the time period of 200 min. As compared to that of pure ZnO, the higher photocatalytic activities

and degradation coefficient of the S-Cl doped ZnO photocatalysts was observed, depicting the enhancement effect of S-Cl doping on performance of ZnO photocatalysts. The obtained findings of the degradation efficiency for the (5, 10, 15) mg S-Cl doped ZnO catalysts had to be achieved 99.66%, 76.67%, 63.28%, respectively as shown in Fig 11(c). As for as the degradation rate constant at the different concentration of MB is concerned we have employed equation 12 to deduce the reaction constant. The operation of slope over the graph between $Ln \frac{C_0}{C_t}$ and time yielded the K value known as degradation constant as shown in Fig.12 (b). The obtained value were found to have been equal to 0.01744, 0.01162, 0.00608 min^{-1} for $(0.62, 1.87 \text{ and } 2.50) \times 10^{-6} \text{M}$ respectively, indicating the degradation activity decreases as MB concentration increases as shown in Fig 13 (b). Fig 12 (a) shows the graph C_t/C_0 versus time indicating the decreasing trend of degradation over the time period of 150 min for S-Cl doped ZnO. The effect of MB concentration on the degradation efficiency was observed in inverse relation. The obtained values for the degradation efficiency were 95.46, 80.15, 65.56% for the $(0.62, 1.87 \text{ and } 2.50) \times 10^{-6} \text{M}$ MB respectively. The findings of degradation efficiency are in line with the previous studies [52, 53]. The maximum degradation rate constant was obtained 0.03188 min^{-1} for 15 mg by loading of photocatalyst which is almost 13.74 times of pristine ZnO. The degradation efficiency of S-Cl doped ZnO was obtained almost 100%, which is almost 2.36 times of pristine ZnO. The enhanced photocatalytic efficiency was attributed to multi approaches reported in the previous studies [45, 46, 52-53]. In addition, the band gap of pristine ZnO and S-Cl doped ZnO play influential role in enhancing photocatalytic activity for the MB. The previous research reveals that lowering the band gap is proportional to the mineralization of MB. In our case the nonmetal doping such as S-Cl into ZnO caused the reduction in band gap from 3.25 eV to 2.9 eV which attributed incorporation of S and Cl in lattice of ZnO [54]. The band gap findings are summarized in table 2, whereas the degradation efficiency and rate coefficient findings are tabulated in Table 3. Moreover, the recent literature survey reveals that numerous oxidants such as peroxymonosulfate, hydrogen peroxide (H_2O_2), peroxydisulfate, ClO_3^- etc. in heterogeneous photocatalytic system may lead to the increase in the degradation efficiency following either by limiting e^-/h^+ recombination rate with the generation of superoxide radical ion ($\text{O}_2^{\bullet-}$) by the capturing of conduction band electrons at the surface of ZnO photocatalyst or by providing additional oxygen atoms acting as an agent to capture electron [55]. Herein, reports of previous study on the effect of varying dose of oxidant H_2O_2 (5 – 30 m mol) revealed that addition of H_2O_2 into thin film N-doped ZnO/CNT

nanocomposite photocatalyst increase the degradation efficiency for the removal of MB dye in the presence of UV light irradiation [56,57]. The oxidant H_2O_2 may be considered the responsible for the formation of highly reactive radical intermediates and the electron capturing agents. Consequently, the concentration of $\bullet OH$ radicals may be increased by the addition of H_2O_2 to the heterogeneous system.

4. Conclusions

In summary, photocatalytic performance of the hydrothermally synthesized non-metal S-Cl doped ZnO and pristine ZnO nanostructures have been reported. The characterizing techniques such as SEM mapping, XRD and EDS, TEM were used to elucidate the structure, morphology, composition and crystal information. The optical band of ZnO was dropped from 3.25 eV to 2.9 eV with simultaneous doping of S and Cl. The maximum degradation rate constant was obtained 0.03188 min^{-1} for 0.15 mg/L loading of photocatalyst which is almost 15 times of pristine ZnO. The degradation efficiency of 100% for the S-Cl doped ZnO over the time of 150 min was obtained which is almost 2.36 times of pristine ZnO. Thus, S-Cl doped ZnO nanostructures may be considered as the potential photocatalysts for purifying the waste water of textile industry and could be used for other environmental applications.

Acknowledgments

We would like to thank the platform “Microscopies, Microprobes and Metallography (3M)” (Institut Jean Lamour, IJL, Nancy, France) for TEM and SEM facilities and J. Ghanbaja for his valuable help for analysis TEM. A.N and S.S.M extend sincere appreciation to the Researchers Supporting Project (RSP-2021/79) at King Saud University, Riyadh, Saudi Arabia.

Conflict of interest statement

Authors declare no conflict of interest in this study.

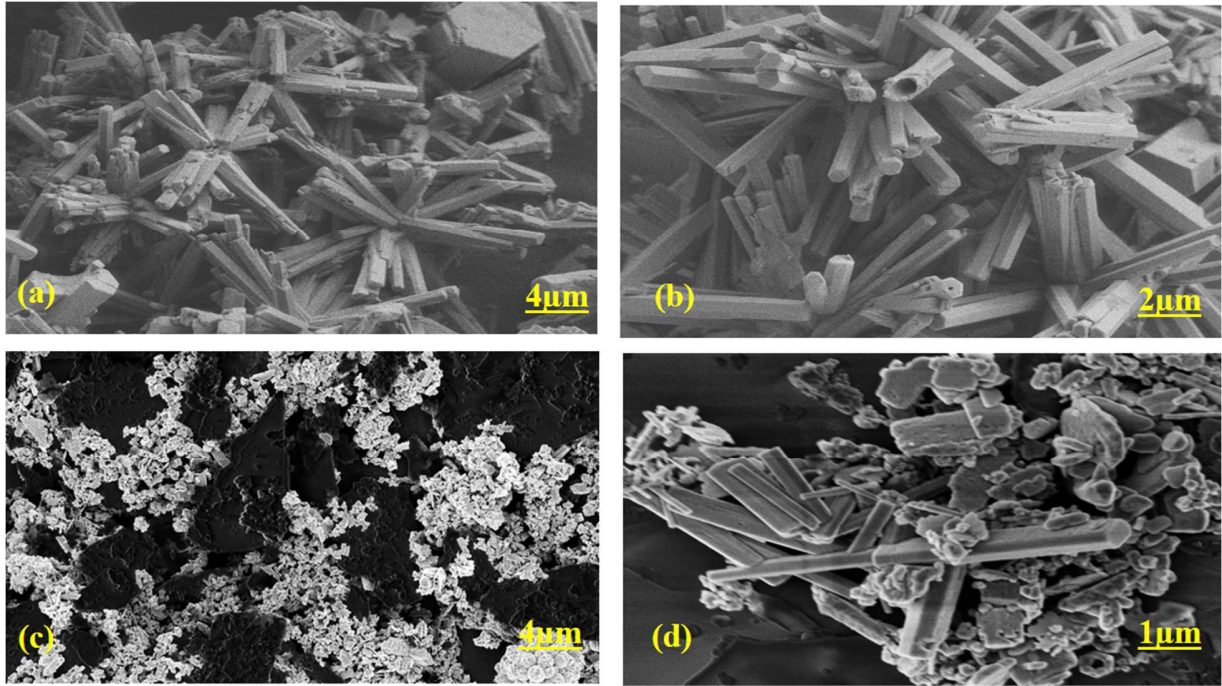


Figure 1: Distinctive SEM images (a-b) Pristine ZnO, (c-d) S-Cl doped ZnO nanostructures

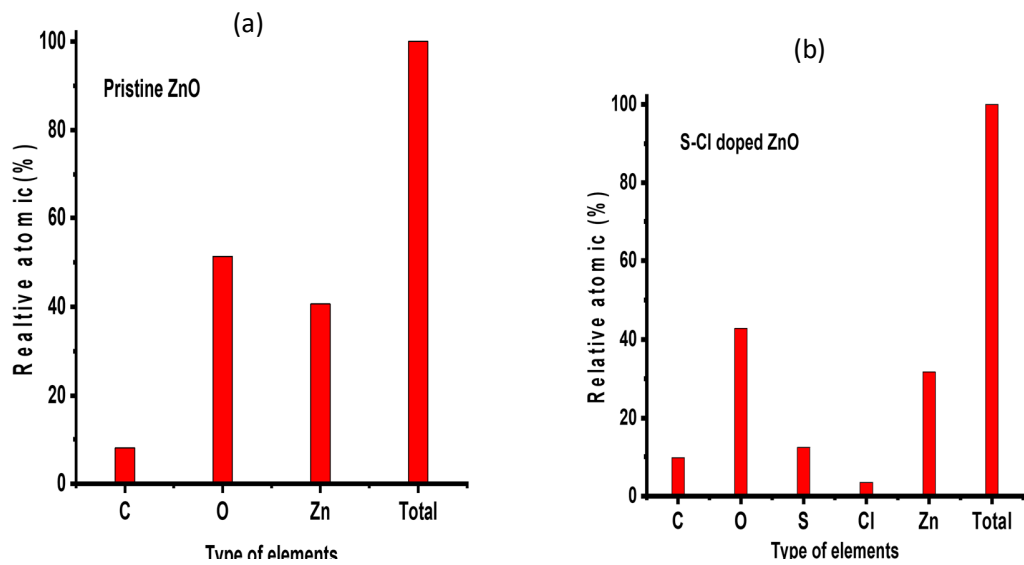


Figure: 2. (a) EDS shows the ingredients of pristine ZnO (b) shows the ingredients of S-Cl doped ZnO

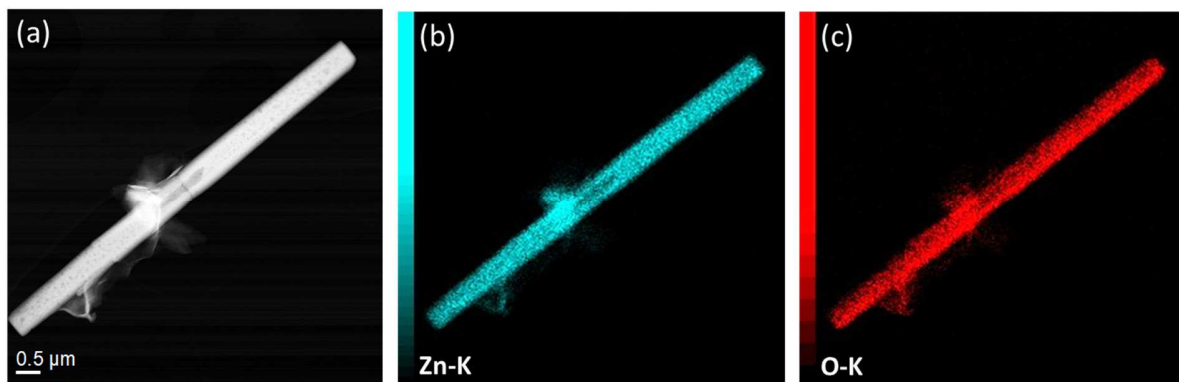


Figure 3: STEM HAADF (a) image and corresponding X-maps of Zn (b) and O (c) elements for the pristine ZnO sample.

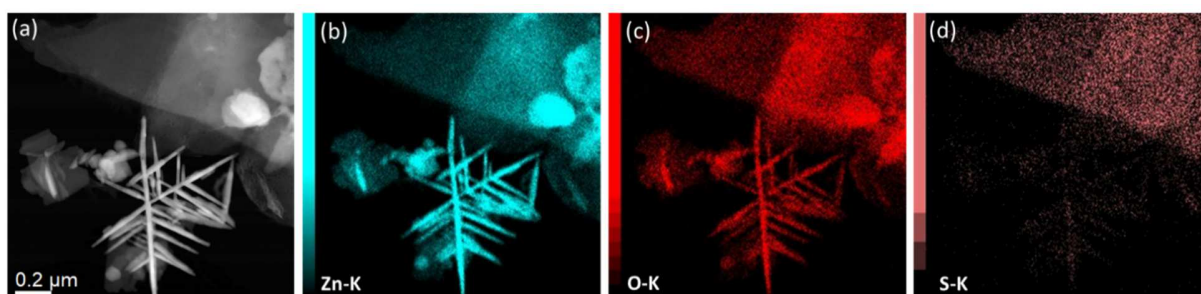


Figure 4: STEM HAADF (a) image and corresponding X-maps of Zn (b), O (c) and S (d) elements for the S-Cl doped ZnO sample.

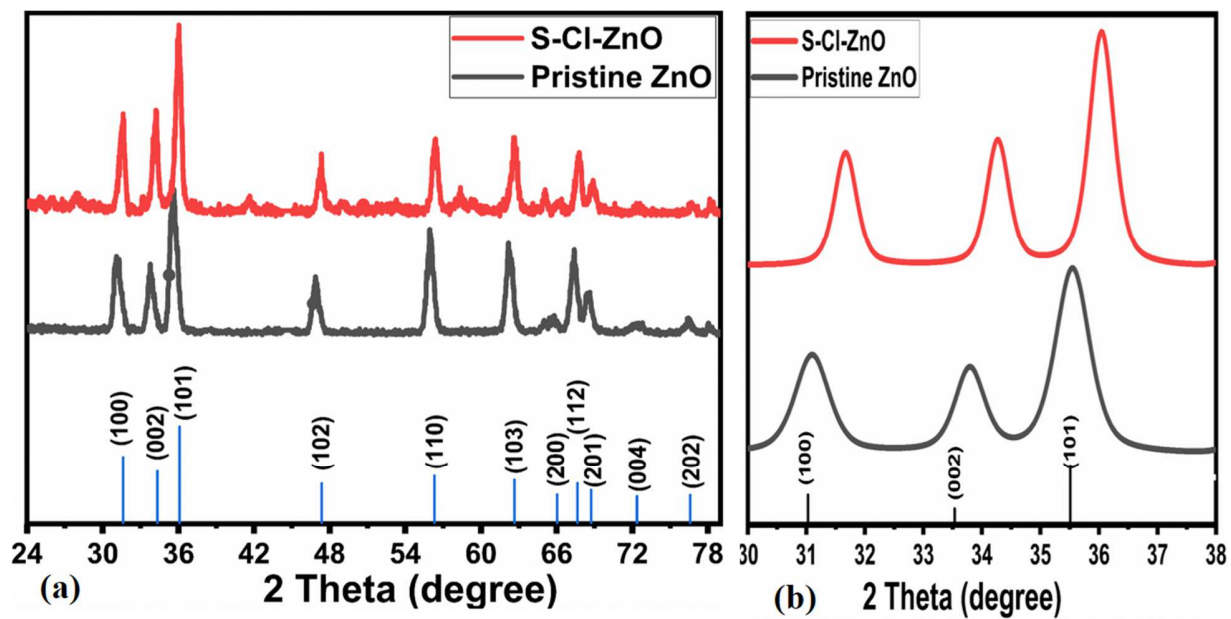


Figure 5. (a) shows XRD patterns for pure and S-Cl-doped ZnO nanostructures, which can be marked as a single phase of wurtzite ZnO structure (b) shows increasing shift in peak at 2Theta angle of 31.17, 33.58, 35.68 degree.

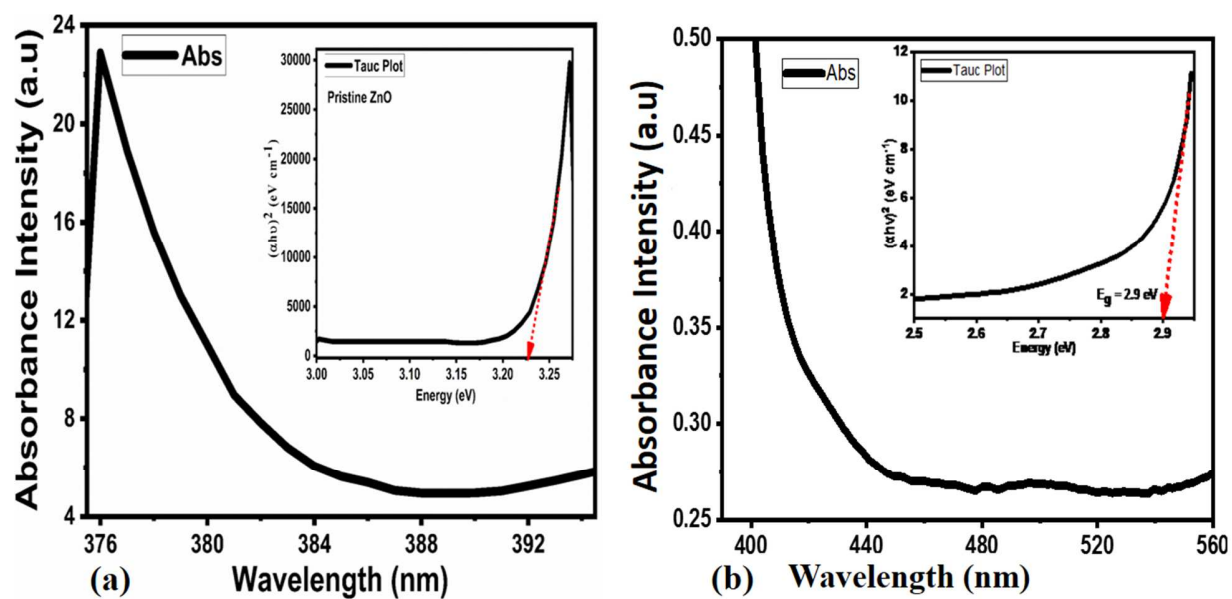


Figure: 6. (a-b) shows findings of the band gap of Pristine ZnO and S-Cl doped ZnO deduced from recording the UV-vis spectrum.

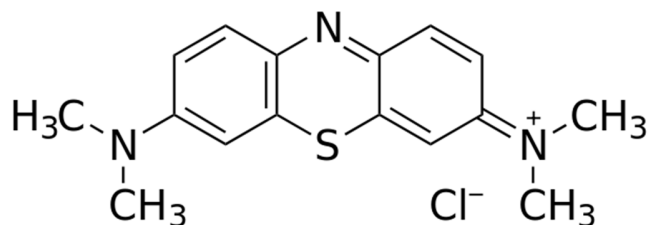


Figure: 7. Chemical Structure of Methyl Blue

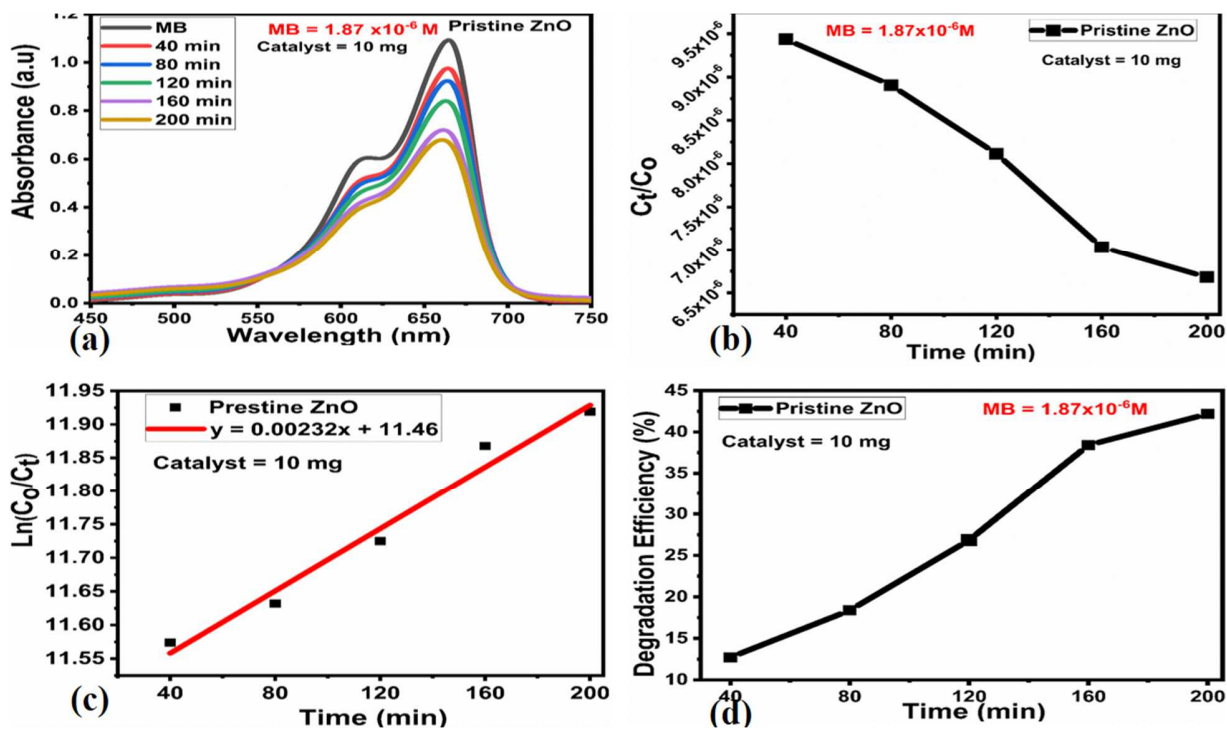


Figure: 8. (a) UV-Vis absorbance spectrum of MB at certain intervals for Pristine ZnO (b) depicts C_t/C_0 versus time (c) linearly fitted graph $\ln(C_0/C_t)$ versus time showing degradation rate.

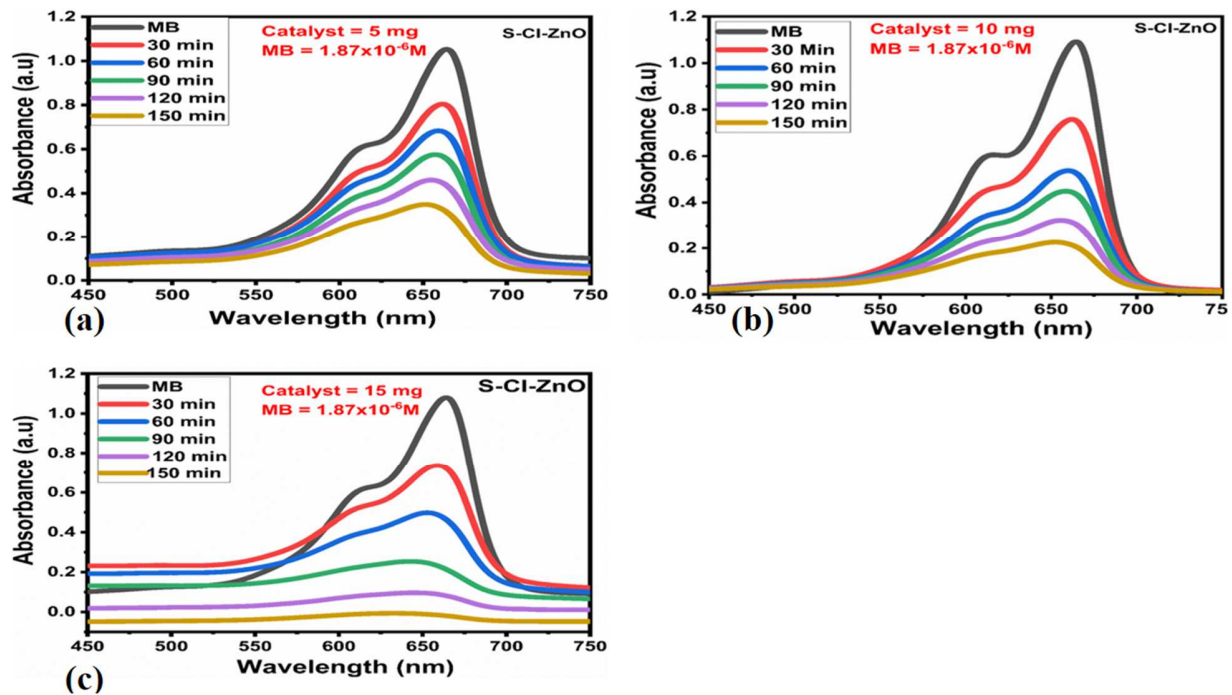


Figure: 9. (a-c) UV-Vis absorption spectrum of MB = $1.87 \times 10^{-6} \text{ M}$ at different concentration of photocatalyst 5, 10 and 15mg.

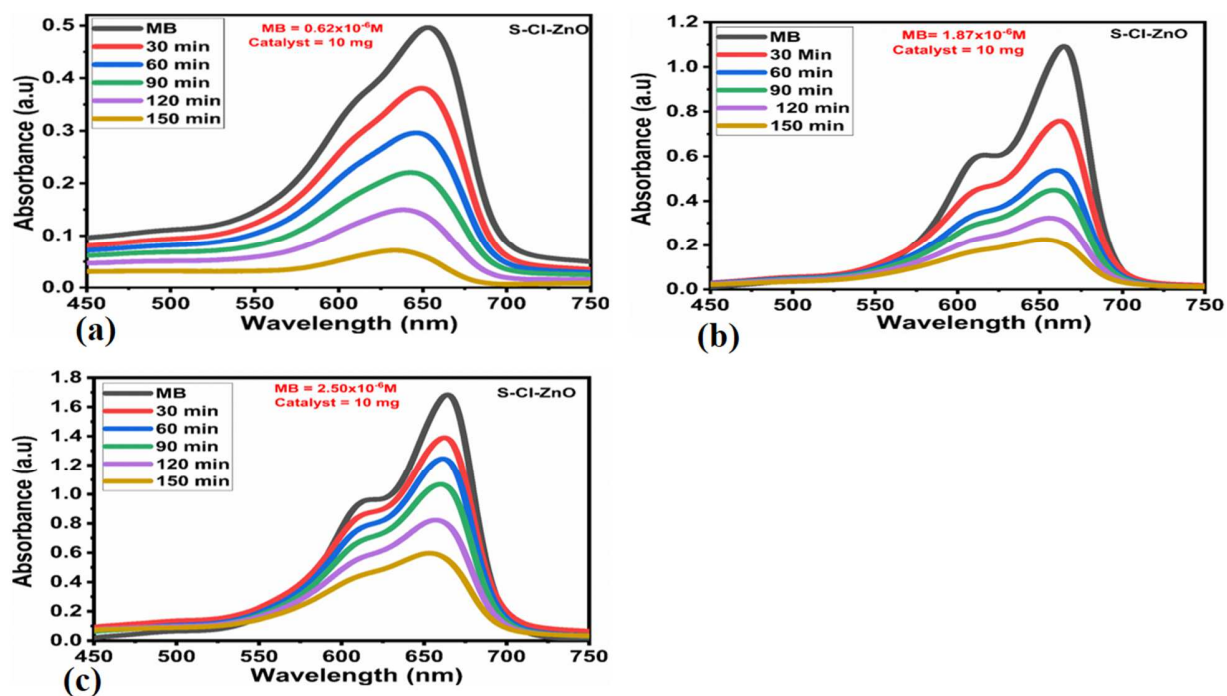


Figure: 10. (a-c) showing UV-Vis absorption spectrum for the different concentration of MB Dye (0.62 , 1.87 and 2.50) $\times 10^{-6}$ M at photocatalyst loading of 10 mg.

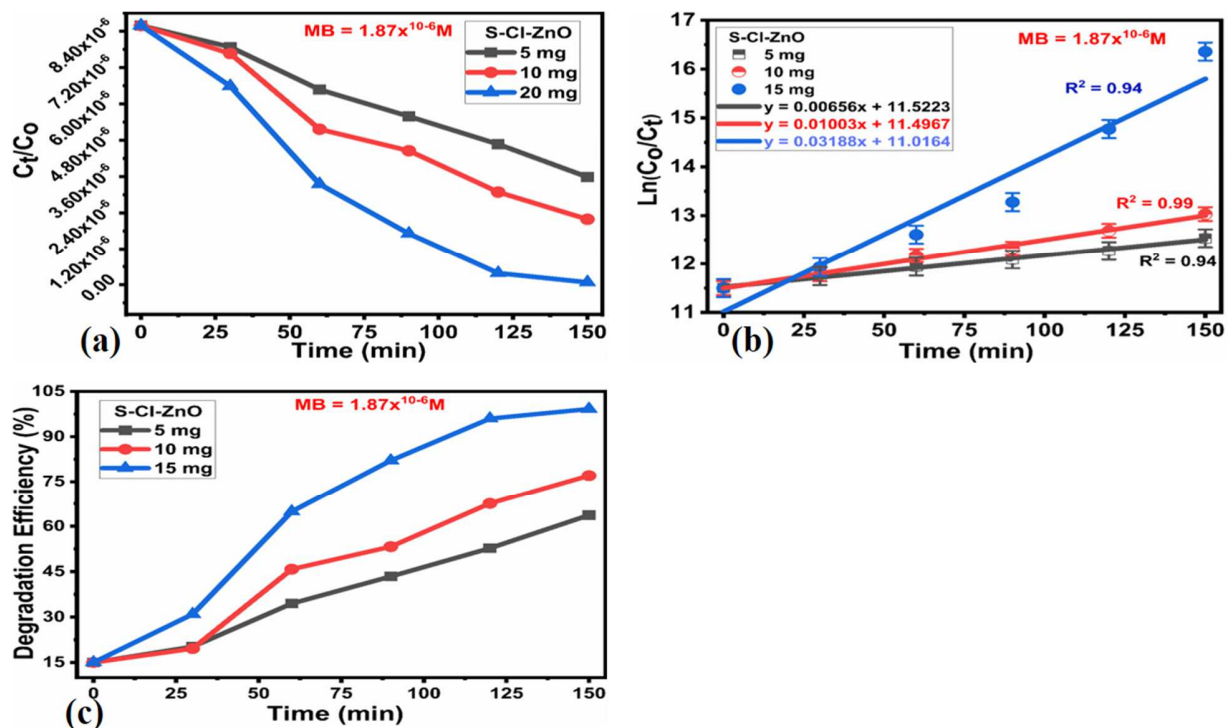


Figure: 11. (a) Depicts graph C_t/C_0 versus time indicating decreasing trend for (5, 10 and 15 mg) of S-Cl-ZnO at $1.87 \times 10^{-6} \text{ M}$ of MB (b) linearly fitted graph $\ln(C_0/C_t)$ versus time showing increasing degradation rate for (5, 10 and 15 mg) of S-Cl-ZnO (c) Photodegradation Efficiency of S-Cl-ZnO nanostructures at (5, 10 and 15 mg)

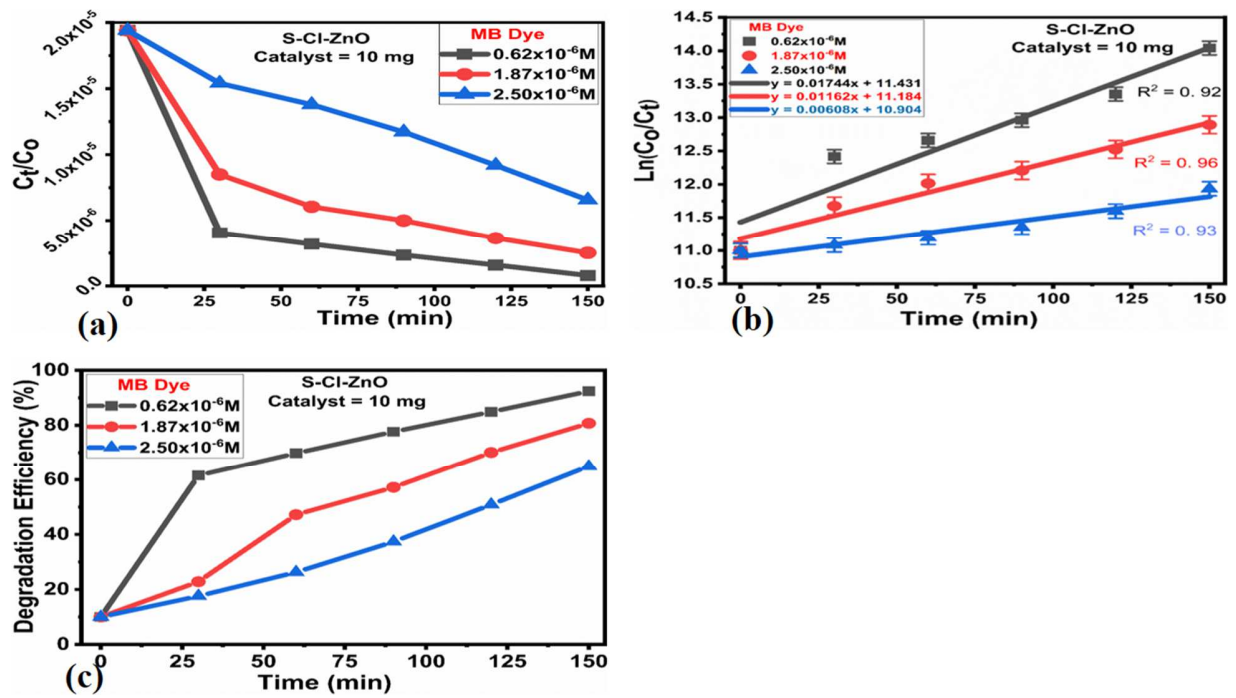


Figure: 12. (a) Depicts graph C_t/C_0 versus time indicating decreasing trend for $(0.62, 1.87 \text{ and } 2.50) \times 10^{-6} \text{ M}$ for 10 mg of S-Cl-ZnO (b) linearly fitted graph $\ln(C_0/C_t)$ versus time showing increasing

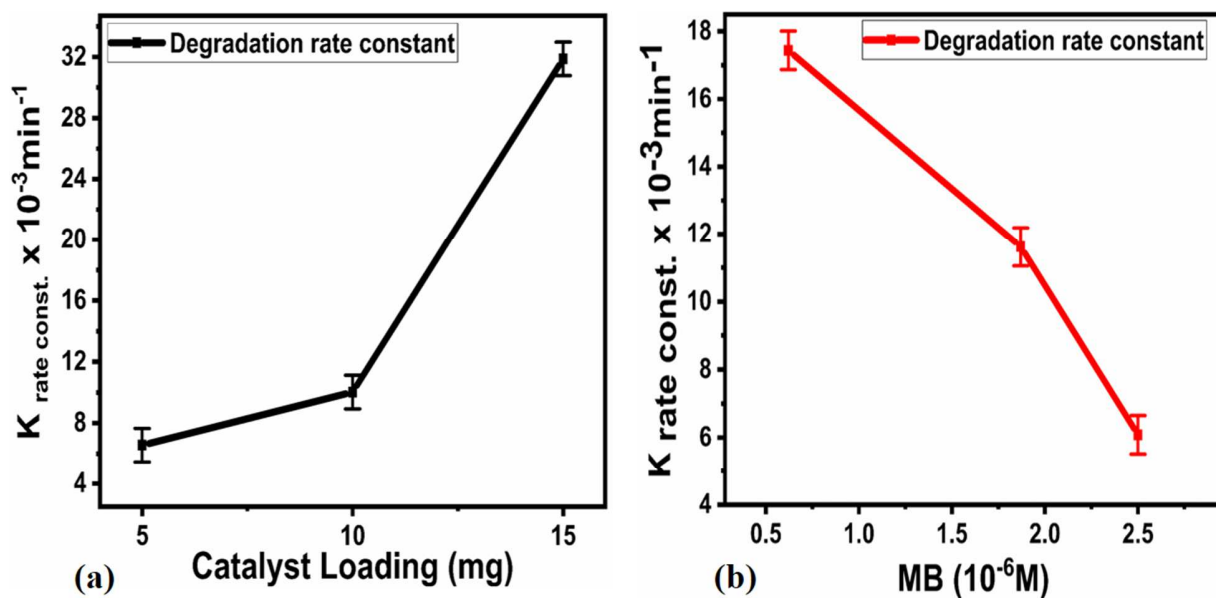


Figure: 13. (a) Degradation rate constant for different catalyst loadings (b) Degradation rate constant for varying MB dye concentration

Table 1:Crystal Parameters of Pristine ZnO as well as S and Cl doped ZnO Nanostructures.

Index	Parameters	Pristine ZnO			S-Cl-ZnO		
1	Crystalline Plane	(100)	(101)	(110)	(100)	(101)	(110)
2	2 θ (Degree)	31.0869	35.6364	55.9486	31.7745	36.0246	56.3820
3	FWHM (degree)	0.45938	0.6200	0.3971	0.6201	0.5377	0.6830
4	Maximum Height	191.328	94.304	121.930	210.469	102.774	157.540
5	Crystalline Size (nm)	35.292	50.2117	42.1591	26.2092	44.4225	23.4961
6	d-spacig (\AA)	4.7324	0.9032	1.8822	4.3458	1.0433	6.6916

Table 2: Band gap of Pristine ZnO and S-Cl doped ZnO Nanostructures.

Samples	Band Gap (eV)
Pristine ZnO	3.25
S-Cl-ZnO	2.90

Table 3: Photocatalytic degradation rate constant (k) and Degradation efficiency, Regression Coefficient for different catalyst loading and different methyl blue under UV radiation.

Catalyst	Different Catalyst Loading (mg) at 1.87×10^{-6} M of MB	5	10	15
S-Cl-ZnO	$K_{rate\ constant} \times 10^{-3} \text{min}^{-1}$	6.56	10.03	31.88
	Regression Coefficient (R^2)	0.99	0.99	0.94
	Degradation Efficiency (%)	63.28	76.67	99.66
	Initial conc. of MB dye ($\times 10^{-6}$ M) at 10mg of catalyst	0.62	1.87	2.5
	$K_{rate\ constant} \times 10^{-3} \text{min}^{-1}$	17.44	11.62	6.08
	Regression Coefficient (R^2)	0.92	0.96	0.93
	Degradation Efficiency (%)	93.46	80.15	65.56

References:

- [01] S. Gita, A Hussan, T.G. Choudhury; Impact of Textile Dyes Waste on Aquatic Environments and its Treatment, *J. Chem.Sci.* (2017), 8, 162-166,
- [02] M Ali, T..R. Sreekrishna, Aquatic Toxicity From Pulp and Paper Mill Effluents: A Rev. *Advan. in Environ. Res.* 2001, 5, 175-196,
- [03] L. Anju Chanua, W. Joychandra Singha, K. Jugeshwar Singhb, K. Nomita Devi; Effect of operational parameters on the photocatalytic degradation of Methylene blue dye solution using manganese doped ZnO nanoparticles; *Results in Physics* 12 (2019) 1230–1237,
- [04] B. Viswanathan, Photocatalytic Degradation of Dyes: An Overview. *Curr. Catal.*, Volume7, Number2,(2018),pp. 99-121(23),
- [05] A. N. Rao, B. Sivasankar, V Sadasivam, Kinetic studies on the photocatalytic degradation of Direct Yellow12 in the presence of ZnO catalyst. *J Mol Catal A: Chem* (2009);306:77–81
- [06] S.A Ansari, S.G Ansari, H Foad.,; M.H Cho, Facile and sustainable synthesis of carbon-doped ZnO nanostructures towards the superior visible light photocatalytic performance. *New J. Chem.* (2017), 41,9314–9320.
- [07] R. Sedghi, F. Heidari, A novel & effective visible light-driven TiO₂/magnetic porous graphene oxide nanocomposite for the degradation of dye pollutants. *RSC Adv.* (2016), 6, 49459–49468.
- [08] S Balu.,; K Uma, G.T Pan, T.C.K. Yang, S.K Ramaraj,. Degradation of methylene blue dye in the presence of visible light using SiO₂@_Fe₂O₃ nanocomposites deposited on SnS₂ flowers. *Materials* (2018), 11, 1030
- [09] K Loh.,; C.C Gaylarde.,; M.A Shirakawa, Photocatalytic activity of ZnO and TiO₂ ‘nanoparticles’ for use in cement mixes. *Constr. Build. Mater.* (2018), 167, 853–859,
- [10]. D. Saravanakkumar, H.A Oualid.,; Y Brahmi.,; A. Ayeshamariam,; M Karunanaithy.,; A.M. Saleem, K. Kaviyarasu, S. Sivaranjani, M Jayachandran, Synthesis and characterization of CuO/ZnO/CNTs thin films on copper substrate and its photocatalytic applications. *OpenNano* (2019), 4, 100025
- [11]. A. Zyoud, N. Zaatar, I. Saadeddin, M.H. Helal,; G. Campet, M. Hakim, D. Park, H.S. Hilal, Alternative natural dyes in water purification: Anthocyanin as TiO₂-sensitizer in methyl orange photo-degradation, *Solid State Sci.* (2011), 13, 1268–1275,
- [12] G. Elango, S.M Roopan, Efficacy of SnO₂ nanoparticles toward photocatalytic degradation of methylene blue dye. *J. Photochem. Photobiol. B Biol.* (2016), 155, 34–38.
- [13] S. Ameen, M. S. Akhtar, H. K. Seo, and H. S. Shin, Solution-processed CeO₂/TiO₂ nanocomposite as potent visible light photocatalyst for the degradation of bromophenol dye, *Chem. Eng. J.* (2014),247, 193–198
- [14] Das, A.; Malakar, P.; Nair, R.G. Engineering of ZnO nanostructures for efficient solar photocatalysis. *Mater. Lett.* (2018), 219, 76–80.
- [15] J.Schumann, M Eichelbaum, T Lunkenbein, N. Thomas, M.C Álvarez Galván, R. Schlögl, M. Behrens, Promoting Strong Metal Support Interaction: Doping ZnO for Enhanced Activity of Cu/ZnO:M (M = Al, Ga, Mg) Catalysts. *ACS Catal.* (2015), 5, 3260–3270.
- [16]. V. Kumari, A. Mittal, J Jindal, S. Yadav, N. Kumar, S-, N- and C-doped ZnO as semiconductor photocatalysts: A review. *Front. Mater. Sci.* (2019), 13, 1–22.
- [17]. T.C. Bharat, S. Mondal, H.S Gupta. P.K Singh,. A.K Das, Synthesis of Doped Zinc Oxide Nanoparticles: A Review. *Mater. Today Proc.* (2019), 11, 767–775.

- [18]. U. Poornaprakash, K. Chalapathi, S.V. Subramanyam, Y. Prabhakar Vattikuti, S.P. Shun, Effects of Ce incorporation on the structural, morphological, optical, magnetic, and photocatalytic characteristics of ZnO nanoparticles. *Mater. Res. Express* (2019), 6, 105356.
- [19]. B. Poornaprakash, K. Subramanyam, S.V.P. Vattikuti, M.S. Pratap Reddy, Achieving enhanced ferromagnetism in ZnTbO nanoparticles through Cu co-doping. *Ceram. Int.* (2019), 45, 16347–16352.
- [20]. B. Poornaprakash, U. Chalapathi, P.T Poojitha, S.V.P Vattikuti, M.S.P. Reddy, (Al, Cu) Co-doped ZnS nanoparticles: Structural, chemical, optical, and photocatalytic properties. *J. Mater. Sci. Mater. Electron.* (2019), 30, 9897–9902.
- [21]. M. Kaur, A. Umar, S.K. Mehta, S. Singh, S.K. Kansal, H. Fouad, O.Y. Allothman, Rapid Solar-Light Driven Superior Photocatalytic Degradation of Methylene Blue Using MoS₂-ZnO Heterostructure Nanorods Photocatalyst. *Material* (2018), 11, 2254.
- [22]. W. Vallejo, C. Díaz-Uribe, K. Rios, Methylene Blue Photocatalytic Degradation under Visible Irradiation on In₂S₃ Synthesized by Chemical Bath Deposition. *Adv. Phys. Chem.* (2017), 2017, 1–5.
- [23]. B. Subash, B. Krishnakumar, M. Swaminathan, M. Shanthi, Highly Efficient, Solar Active, and Reusable Photocatalyst: Zr-Loaded Ag–ZnO for Reactive Red 120 Dye Degradation with Synergistic effect and Dye-Sensitized Mechanism. *Langmuir* (2013), 29, 939–949.
- [24]. H. Aby, A. Kshirsagar, K. Pk, Plasmon Mediated Photocatalysis by Solar Active Ag/ZnO Nanostructures: Degradation of Organic Pollutants in Aqueous Conditions. *J. Mater Sci Nanotechnol* (2016), 4.
- [25]. C. Díaz-Uribe, J. Vilorio, L. Cervantes, W Vallejo, K. Navarro, E. Romero, C. Quiñones, Photocatalytic Activity of Ag-TiO₂ Composites Deposited by Photoreduction under UV Irradiation. *Int. J. Photoenergy* (2018), 2018, 1–8.
- [26]. L. Chen, T.T. Tran, C. Huang, J. Li, L. Yuan, Q. Cai, Synthesis and photocatalytic application of Au/Ag nanoparticle-sensitized ZnO films. *Appl. Surf. Sci.* (2013), 273, 82–88.
- [27]. B. Poornaprakash, U. Chalapathi, P.T Poojitha, S.V.P Vattikuti, S.H. Park, Co-Doped ZnS Quantum Dots: Structural, Optical, Photoluminescence, Magnetic, and Photocatalytic Properties. *J. Supercond. Nov. Magn.* (2020), 33, 539–544.
- [28]. Z. Youssef, L. Colombeau, N. Yesmurzayeva, F. Baros, R. Vanderesse, T. Hamieh, J. Toufaily, C. Frochot, T. Roques-Carmes, S. Acherar, Dye-sensitized nanoparticles for heterogeneous photocatalysis: Cases studies with TiO₂, ZnO, fullerene and graphene for water purification. *Dye Pigment.* (2018), 159, 49–71.
- [29]. W Vallejo, C. Diaz-Uribe, Á. Cantillo, Methylene blue photocatalytic degradation under visible irradiation on TiO₂ thin films sensitized with Cu and Zn tetracarboxyphthalocyanines. *J. Photochem. Photobiol. A Chem.* (2015), 299, 80–86.
- [30]. W. Vallejo, A. Rueda, C. Díaz-Uribe, C. Grande, P. Quintana, Photocatalytic activity of graphene oxide–TiO₂ thin films sensitized by natural dyes extracted from *Bactris guineensis*. *R. Soc. Open Sci.* (2019), 6, 181824.
- [31]. C. Diaz-Uribe, W. Vallejo, G. Camargo, A. Muñoz-Acevedo, C. Quiñones, E. Schott, X. Zarate, Potential use of an anthocyanin-rich extract from berries of *Vaccinium meridionale* Swartz as sensitizer for TiO₂ thin films—An experimental and theoretical study. *J. Photochem. Photobiol. A Chem.* (2019), 384, 112050
- [32]. S.B.A. Hamid, S.J Teh, C.W Lai, Photocatalytic Water Oxidation on ZnO: A Review. *Catalysts* (2017), 7, 93.

- [33] S.,S. Türkyılmaz, N. Güy, M. Özacar, Photocatalytic efficiencies of Ni, Mn, Fe and Ag doped ZnO nanostructures synthesized by hydrothermal method: The synergistic/antagonistic effect between ZnO and metals. *J. Photochem. Photobiol. A Chem.* (2017), 341, 39–50.
- [34] L.-C. Chen, Y.-J. Tu, Y.-S. Wang, R.-S. Kan, and C.-M. Huang, “Characterization and photoreactivity of N-, S-, and C-doped ZnO under UV and visible light illumination,” *Journal of Photochemistry and Photobiology A: Chemistry*, vol. 199, no. 2-3, (2008) pp. 170–178,
- [35] S. Liu, C. Li, J. Yu, and Q. Xiang, “Improved visible-light photocatalytic activity of porous carbon self-doped ZnO nanosheet assembled flowers,” *CrystEngComm*, vol. 13, no. 7, (2011) pp. 2533–2541.
- [36] A. B. Lavand and Y. S. Malghe “Synthesis, Characterization, and Visible Light Photocatalytic Activity of Nanosized Carbon Doped Zinc Oxide” *International Journal of Photochemistry Volume* (2015) Article ID 790153, 9 pages
- [37] S.Z. Kang, T Wu, X Li, J Mu, A facile gelatin-assisted preparation and photocatalytic activity of zinc oxide nanosheets. *Colloids and Surfaces A: Physicochemistry and Engineering Aspects* 369(1-3): (2010) 268-271.
- [38] K. Gautam, I. Singh, P.K. Bhatnagar, K. Rao Peta1 “Role of Cl Doping on the Growth and Relaxation Dynamics of ZnO Nanorods Synthesized by Hydrothermal Method” *Chemical Physics Letters* (2016) S0009-2614(16)30700-X
- [39] A. Jiamprasertboon, C. S. Dixon, S. Sathasivam, M. J. Powell, Y. Lu, T. Siritanon and C. J. Carmal, “Low-Cost One-Step Fabrication of highly Conductive ZnO:Cl Transparent Thin Films with Tunable Photocatalytic Properties via Aerosol-Assisted Chemical Vapor Deposition” *ACS Applied Electronic Materials* (2019) 1408-1417
- [40] Y. Xu, J. Zou, X. Lin, W. Wu, W. Li, B. Yang, M. Shi, Quality-Improved GaN Epitaxial Layers Grown on Striped Patterned Sapphire Substrates Ablated by Femtosecond Laser. *Appl. Sci.* (2018), 8, 1842
- [41] T. T. Loan Nguyen, Lan T. H. Nguyen, Anh T. T. Duong, Bui Duc Nguyen, Nguyen Quang Hai, Viet Ha Chu, Trinh Duy Nguyen, and Long Giang Bach “Preparation, Characterization and Photocatalytic Activity of La-Doped Zinc Oxide Nanoparticles, *Materials* (2019), 12, 1195; doi:10.3390/ma12081195
- [42] G. E. Lau, C. Azurahaman, C. Abdullah, W. Amir N. Wan Ahmad, S. Assaw and A. L. Teik Zheng Eco-Friendly Photocatalysts for Degradation of Dyes, *Catalysts* (2020), 10, 1129
- [43] A. Jiamprasertboon, S. C. Dixon, S. Sathasivam, M. J. Powell, Yao Lu, T. Siritanon, and C. J. Carmal, “Low-Cost One-Step Fabrication of Highly Conductive ZnO:Cl Transparent Thin Films with Tunable Photocatalytic Properties via Aerosol-Assisted Chemical Vapor Deposition” *ACS Applied Electronic Materials* (2019) 1408-1417
- [44] T. Xia, Y.L Zhang, J. Murowchick, X.B. Chen, Vacuum-treated titanium dioxide nanocrystals: Optical properties, Surface disorder, oxygen vacancy, and photocatalytic activities. *Catal. Today* (2014), 225, 2–9.
- [45] Senthilvelan S, Chandraboss VL, Karthikeyan B, Natanapatham 498 L, Murugavelu M 484 TiO₂, ZnO and nanobimetallic silica catalyzed photodegradation of methylgreen. *Mater. Sci. 485 Semicond Process* (2013) 16:185–192

- [46] H Xu, T Yu, J Liu Photo-degradation of Acid Yellow 11 in aqueous on nano ZnO/Bentonite under ultraviolet and visible light irradiation. *Mat Letters*, (2014)117: 263–265
- [47] A Balcha, OP Yadav, T Dey Photocatalytic degradation of methylene blue dye by zinc oxide nanoparticles obtained from precipitation and sol-gel methods. *Environ Sci Pollut Res* (2016) 23:25485–25493.
- [48] R Malik, V. Chaudhary, V.K Tomer, P.S. Rana, S.P. Nehra, Visible light-driven mesoporous Au–TiO₂/SiO₂ photocatalysts for advanced oxidation process. *Ceram. Int.* (2016), 42, 10892–10901.
- [49] A. Hassani, A. Khataee, S. Karaca, C. Karaca, P. Gholami, Sonocatalytic degradation of ciprofloxacin using synthesized TiO₂ nanoparticles on montmorillonite. *Ultrason. Sonochem.* (2017), 35, 251–262
- [50] N. Perciani, D. Moraes, F. Nascimento, M. Lucia, C. Pinto, T. Moreira, B. Campos, G.P. Thim, L.A. Rodrigues, Methylene blue photodegradation employing hexagonal prism-shaped niobium oxide as heterogeneous catalyst: Effect of catalyst dosage, dye concentration, and radiation source. *Mater. Chem. Phys.*(2018), 214, 95–106.
- [51] S. G. Shelar, V. K. Mahajan, S. P. Patil, G. H. Sonawane; Effect of doping parameters on photocatalytic degradation of methylene blue using Ag doped ZnO nanocatalyst; *SN Applied Sciences* (2020) 2:820
- [52] S. Chakrabarti, B.K. Dutta Photocatalytic degradation of model textile dyes in wastewater using ZnO as semiconductor catalyst. *J Hazard Mater* 112(3): (2004)269–278
- [53] N. Soltani, E Saion, M.Z Hussein, M Erfani, A Abedini, G Bahmanrokh, M Navasery, P Vaziri , Visible light-induced degradation of methylene blue in the presence of photocatalytic ZnS and CdS nanoparticles. *Int J Mol Sci* 13: (2012) 12242–12258
- [54] M.A. Bhatti, A. A. Shah, K. F. Almani, A. Tahira, S. E. Chalangar, A. D. Chandio, O. Nur, M. Willander, Z. H. Ibupoto; Efficient photo catalysts based on silver doped ZnO nanorods for the photo degradation of methyl orange, *Ceramics International* 45 (2019) 23289–23297
- [55] M.A. Subhan, M.R. Awal, T. Ahmed, M. Younus, Photocatalytic and Antibacterial activities of Ag/ZnO Nanocomposites Fabricated by Co-Precipitation Method. *Acta Metall. Sin. (Engl. Lett.)* (2014), 27, 223–232.
- [56] T. Lv, L. Pan, X. Liu, T. Lu, G. Zhu, Z. Sun, Enhanced photocatalytic degradation of methylene blue by ZnO-reduced graphene oxide composite synthesized via microwave-assisted reaction. *J. Alloys Compd.*, 509, (2011)10086–10091.
- [57] M. Elias, M. N. Uddin, J. K. Saha, M. A. Hossain, D. R. Sarker, S. Akter, I. A. Siddiquey and J. Uddin; A Highly Efficient and Stable Photocatalyst; N-Doped ZnO/CNT Composite Thin Film Synthesized via Simple Sol-Gel Drop Coating Method, *Molecules* (2021), 26, 1470

